

SEARCHING FOR PLANETS IN THE HYADES. III. THE QUEST FOR SHORT-PERIOD PLANETS^{1,2}

DIANE B. PAULSON³

Department of Astronomy, University of Texas at Austin, Austin, TX 78712; apodis@astro.as.utexas.edu

STEVEN H. SAAR

Harvard-Smithsonian Center for Astrophysics, 60 Garden Street, Cambridge, MA 02138; ssaar@cfa.harvard.edu

WILLIAM D. COCHRAN

McDonald Observatory, University of Texas at Austin, Austin, TX 78712; wdc@astro.as.utexas.edu

AND

GREGORY W. HENRY⁴

Center of Excellence in Information Systems, Tennessee State University, 330 10th Avenue North, Nashville, TN 37203; henry@schwab.tsuniv.edu

Received 2003 February 12; accepted 2003 December 3

ABSTRACT

We have been using the Keck I High Resolution Spectrograph to search for planetary companions in the Hyades cluster. We selected four stars from this sample that showed significant radial velocity variability on short timescales to search for short-period planetary companions. The radial velocities of these four stars were monitored regularly with the Hobby-Eberly Telescope for approximately 2 months, while sparse data were also taken over ~ 4 months: we also obtained near-simultaneous photometric observations with one of the automatic photoelectric telescopes at Fairborn Observatory. For three of the stars, we detect photometric variability with the same period present in the radial velocity (v_r) measurements, compatible with the expected rotation rates for Hyades members. The fourth star continues to show v_r variations and minimal photometric variability but with no significant periodicity. This study shows that for the three stars with periodic behavior, a significant portion of the v_r fluctuations are likely due primarily to magnetic activity modulated by stellar rotation rather than planetary companions. Using simple models for the v_r perturbations arising from spot and plage, we demonstrate that *both* are likely to contribute to the observed v_r variations. Thus, simultaneous monitoring of photometric (photospheric) and spectroscopic (chromospheric) variations is essential for identifying the cause of Doppler-shifted absorption lines in more active stars.

Key words: open clusters and associations: individual (Hyades) — planetary systems: general — stars: activity — stars: spots — techniques: photometric — techniques: radial velocities

1. INTRODUCTION

It is well known that starspots will cause shifts in line profile shapes (cf. Vogt, Penrod, & Hatzes 1987), which will cause apparent Doppler shifts of the lines. Saar & Donahue (1997) modeled the expected v_r variability due to the rotational modulation of spots. Hatzes (1999, 2002) makes similar calculations and obtains the same results as Saar & Donahue (1997). Recently, observational data to support this has been published. Queloz et al. (2001) found HD 166435 to have a large velocity amplitude, but it turned out also to show sinusoidal photometric amplitude in Strömgren y with the same period. In addition, the calcium HK index varied smoothly on the same timescale. This indicated the v_r variations were most likely due to stellar activity rather than a planetary companion.

Henry, Donahue, & Baliunas (2002) showed starspots to be the cause of the line shifts in HD 192263, and G. W. H. and P. Butler see the same thing in HD 19632 (G. W. Henry & P. Butler 2002, private communication). Additionally, Saar, Butler, & Marcy (1998) and Santos et al. (2000) confirm the models presented by Saar & Donahue (1997).

The amplitude of v_r caused by plage regions is also beginning to be modeled (Saar 2003). He finds that this can be several tens of meters per second. Therefore, it is important that one monitor all aspects of stellar activity when searching for planets, particularly around active stars. Here, we investigate the implications of the rotational modulation of stellar activity on our search for short-period planets in the Hyades.

2. OBSERVATIONS AND ANALYSIS

2.1. Sample

The motivations for the Keck Hyades survey are discussed by Cochran, Hatzes, & Paulson (2002). With a sample of 98 stars, with $[\text{Fe}/\text{H}] = 0.13$ (Paulson, Sneden, & Cochran 2003), we might expect a small number of short-period planets similar to 51 Peg (Mayor & Queloz 1995). From our Keck Hyades sample, we chose four stars for follow-up observations with the Hobby-Eberly Telescope's (HET) High Resolution Spectrograph (HRS) in search of short-period planetary companions. The targets were chosen from a group of stars that showed significant v_r rms on short timescales. Only four

¹ Some data were obtained with the Hobby-Eberly Telescope (HET). The HET is operated by McDonald Observatory on behalf of The University of Texas at Austin, the Pennsylvania State University, Stanford University, Ludwig-Maximilians-Universität München, and Georg-August-Universität Göttingen.

² Additional data presented herein were obtained at the W.M. Keck Observatory, which is operated as a scientific partnership among the California Institute of Technology, the University of California, and the National Aeronautics and Space Administration (NASA). The Observatory was made possible by the generous financial support of the W.M. Keck Foundation.

³ Current address: Department of Astronomy, 830 Dennison Building, University of Michigan, Ann Arbor, MI 48109.

⁴ Senior Research Associate, Department of Physics and Astronomy, Vanderbilt University, Nashville, TN 37235.

TABLE 1
PROGRAM INFORMATION

Star	vB No.	No. v_r Obs.	K (m s^{-1})	P_{rot, v_r} (days)	FAP $_{v_r}$ (%)	No. Phot. Obs.	Δy	$P_{\text{rot}, \text{phot}}$ (days)	FAP $_y$ (%)	No. Hipp. Obs.	$P_{\text{rot}, \text{Hipp.}}$ (days)	FAP $_{\text{HIP}}$ (%)
HIP 13806.....	153	25	46.2	9.42	1.7	14	0.028	9.18	4.3	62	9.60	0.02
HD 26767.....	18	30	51.1	8.65	7.9	12	0.015	8.65	5.9	34
HD 26736.....	15	29	72.5	8.18	1.4	11	0.026	8.44	15.5	102
HD 26756.....	17	24	27.3	12	0.011	44

were observed at this time due to HET scheduling constraints. The image quality of the telescope was being corrected during this time, and although this did not affect the quality of the observations, it placed a magnitude limit on the stars that could be observed. The observed targets are listed in Table 1.

2.2. v_r Measurements

The v_r observations from the Keck High Resolution Echelle Spectrograph (HIRES) are described in full in Cochran et al. (2002). We began regular observations of these four stars from late 2001 December to mid 2002 February (and a few observations of each star taken sporadically during the fall of 2001) with the HRS at the HET (Tull 1998; Cochran et al. 2003). We used the 3" optical fiber feed to the HRS with resolving power $R = 60,000$. We set the 316 g mm^{-1} cross-disperser to central wavelength 5938 Å. This includes almost the entire I_2 region ($\approx 5000\text{--}6200$ Å; I_2 is used as the velocity metric) on one of the CCD chips. Any other configuration would result in spreading the I_2 region over both CCD chips and losing some I_2 information in the gap between CCDs. We manufactured the I_2 gas absorption cell for use in the HRS at the University of Texas, and during these observations, it was run at 60°C.

Each exposure was restricted to 15 minutes in length to reduce velocity smearing due to the Earth's rotation. This limited the signal-to-noise ratio (S/N) but was necessary to obtain high v_r precision (see Paulson et al. 2002). The S/N varied greatly from exposure to exposure due to seeing variations, but all observations had $S/N \geq 200 \text{ pixel}^{-1}$. The CCD images were reduced and extracted using standard IRAF⁵ packages. We use a program called RADIAL (developed at the University of Texas [UT] and McDonald Observatory) to measure precise radial velocities. This program was adapted for use with data from all of the planet search programs affiliated with UT. Brief discussions of the program may be found in Cochran et al. (1997) and Hatzes et al. (2000). The typical velocity precision for observations with the HET HRS is 4–6 m s^{-1} (Cochran et al. 2003). The K amplitudes are listed in Table 1. The K amplitude for HD 26756, which is not found to have significant periodicity, is just defined as one-half of the peak-to-peak variation of the v_r . The v_r data are listed in Table 2.

2.3. Photometric Measurements

Between 11 and 14 nightly photometric observations of each of the four stars were acquired in 2002 February and March with the T12 0.8 m automatic photoelectric telescope (APT) at Fairborn Observatory in the Patagonia Mountains of

southern Arizona.⁶ The T12 APT measures the difference in brightness between a program star and nearby comparison stars in the Strömbergren b and y passbands. The observing procedures and data reduction techniques employed with this APT are identical to those for the T8 0.8 m APT described in Henry (1999). The resulting Strömbergren b and y differential magnitudes were corrected for differential extinction with nightly extinction coefficients and transformed to the Strömbergren system with yearly mean transformation coefficients. The external precision of the differential magnitudes, defined as the standard deviation of a single differential magnitude from the seasonal mean of the differential magnitudes, is typically around 0.0012 mag for this telescope, as determined from observations of pairs of constant stars. Our primary comparison stars for were HD 26737 (for HD 26736), HD 27561 (for HD 26756 and HD 26767), and HD 18579 (for HIP 13806); all three comparison stars are constant to ~ 0.003 mag or better as determined by intercomparison with additional comparison stars. The resulting range in the differential y magnitudes (Δy) of our four program stars are given in Table 1. Photometric data are listed in Table 3.

3. RESULTS

3.1. P_{rot}

We are able to determine the rotational period (P_{rot}) for these stars from both sets of observations, v_r and Δy , independently. We used the method of Horne & Baliunas (1986) for period determination, and all results are listed in Table 1. We independently determined periods from the photometric data using the procedure outlined in Henry et al. (2001), and these periods are as follows: HIP 13806, 9.57 ± 0.18 days; HD 26736, 8.48 ± 0.35 days; and HD 26767, 8.69 ± 0.13 days. These agree with the periods determined by the method of Horne & Baliunas (listed in Table 1). HD 26736, HD 26767, and HIP 13806 all show relatively significant periods in the period analysis, with false alarm probabilities (FAPs) of $\leq 15\%$ (also calculated by the method described in Horne & Baliunas). P_{rot} is also consistent between spectroscopic and photometric data assuring us that the periods derived in v_r are due to rotational modulation of stellar activity. We chose to use P_{rot} determined from v_r to show the phase plots in Figure 1, since there were more data available. We could, equally as well, have chosen to phase the plots according to P_{rot} as derived from the photometry. Zero phase was chosen to be at photometric maximum, which roughly corresponds to the time at which the v_r curve crosses from “blue” to “red.” This is done because photometric maximum is an easily understandable physical event, thus “grounding” the phase

⁵ IRAF is distributed by the National Optical Astronomy Observatory, which is operated by the Association of Universities for Research in Astronomy, Inc., under cooperative agreement with the National Science Foundation (NSF).

⁶ Further information about Fairborn Observatory can be found at <http://www.fairobs.org/>.

TABLE 2
RADIAL VELOCITIES

Star	JD - 2,400,000	v_r (m s ⁻¹)	Uncertainty (m s ⁻¹)	Star	JD - 2,400,000	v_r (m s ⁻¹)	Uncertainty (m s ⁻¹)	
HIP 13806.....	52,262.770111	27.11	6.35	HD 26736.....	52,238.711713	2.63	5.79	
	52,263.768303	8.46	5.56		52,263.619768	-12.31	7.38	
	52,265.558250	-21.27	6.61		52,264.606026	-17.85	5.86	
	52,266.564679	-28.23	6.80		52,265.606621	-19.30	6.01	
	52,269.747800	-65.33	18.06		52,266.597528	72.02	6.38	
	52,270.756446	-9.11	6.52		52,269.584370	-62.45	7.75	
	52,271.754419	1.83	8.31		52,270.823349	-60.25	7.72	
	52,297.687220	-60.20	4.61		52,271.821446	-33.54	7.08	
	52,299.682102	-13.88	4.89		52,272.587749	-16.98	6.58	
	52,300.694922	-20.44	4.46		52,297.754247	-38.71	6.04	
	52,301.692142	22.06	7.63		52,298.738493	28.13	4.79	
	52,302.690889	-10.32	3.82		52,299.731856	51.27	5.45	
	52,303.678815	-44.98	4.75		52,300.743482	-28.87	6.69	
	52,306.669150	-45.84	3.63		52,301.739367	-73.07	9.49	
	52,312.664745	-24.29	7.08		52,302.737520	-45.38	5.23	
	52,313.641222	-22.49	3.22		52,303.724341	-13.08	4.96	
	52,314.656157	-13.03	16.02		52,306.719880	18.78	5.27	
	52,315.627230	-25.59	5.16		52,307.715564	45.90	4.02	
	52,316.642697	-57.75	4.17		52,312.698359	-6.38	4.56	
	52,317.638826	-20.89	5.27		52,313.693807	-33.77	3.38	
	52,318.648681	-6.70	5.12		52,314.702460	4.90	4.38	
	52,319.639116	-9.43	5.11		52,315.681787	48.11	5.03	
	52,320.642096	4.52	5.29		52,316.697637	24.51	4.73	
	52,321.632011	-14.87	5.60		52,317.684034	-25.61	4.63	
	52,322.615422	-39.87	3.69		52,318.693958	-37.56	5.22	
	HD 26767.....	52,199.811224	59.23		5.84	52,319.690237	4.46	4.76
		52,200.812501	-2.48		5.58	52,320.675927	-14.14	4.64
		52,202.803337	-2.36		4.92	52,321.680885	-11.19	6.62
		52,203.814494	8.44		6.58	52,322.667651	-13.24	5.56
		52,236.872727	-6.04		7.40	52,325.671298	-1.74	4.41
		52,237.893749	-26.90		6.69	52,200.796965	-11.69	6.23
		52,252.676137	3.40		9.22	52,202.783532	25.82	6.74
52,253.845854		6.45	5.58	52,203.989956	16.65	7.52		
52,255.835060		-16.65	5.01	52,247.879099	13.27	8.14		
52,261.818689		26.24	7.64	52,249.861960	-19.19	6.70		
52,299.701994		-42.94	5.98	52,252.660236	-8.91	8.12		
52,300.710344		11.01	4.25	52,253.861596	-7.63	7.69		
52,301.708195		23.47	4.49	52,255.851520	-5.29	6.40		
52,302.706162		-30.54	4.56	52,278.591680	16.13	8.26		
52,303.693759		3.89	3.78	52,299.717028	10.40	5.72		
52,306.688347		-25.46	4.00	52,300.725215	-28.88	5.29		
52,307.697467		-39.37	4.80	52,301.721528	-18.92	5.71		
52,312.681499		28.70	4.82	52,302.719726	-17.26	4.65		
52,313.660480		2.78	4.51	52,303.709706	2.60	5.18		
52,314.671760		-1.10	4.39	52,306.703796	-26.66	4.96		
52,315.651757		-14.89	4.96	52,313.677015	15.59	4.35		
52,316.661289		-21.04	4.07	52,314.685147	-13.61	5.33		
52,317.656991		-0.28	5.26	52,315.666452	3.35	4.85		
52,318.663084		35.16	4.12	52,316.679270	-1.12	5.27		
52,319.657755		8.61	4.17	52,317.670296	-16.98	5.36		
52,320.659775		6.29	4.30	52,318.677153	0.27	5.77		
52,321.649747		23.07	4.23	52,319.673016	16.77	5.08		
52,322.634036		1.43	4.13	52,321.664983	25.44	5.34		
52,325.654987		-3.34	4.86	52,322.651275	-1.53	5.26		

plot. The associated v_r plots are only the results of the active regions (photometric variations).

We searched the *Hipparcos* Epoch Photometry Annex (ESA 1997) of each of these stars for periodicity. The period-finding algorithm of Horne & Baliunas (1986) was again used to search for periodicity in the *Hipparcos* data set. When Queloz et al. (2001) studied HD 166435, they noticed that by taking

small sections of their data in time, they were able to recover P_{rot} . However, when taking the entire data set, they saw no obvious signature of P_{rot} . This was an effect of phase shifts as the spots migrated either in longitude with stellar differential rotation or in latitude or appeared or disappeared asymmetrically. HD 26736 and HD 26767 appear to behave like HD 166435 in that the full photometric data set from *Hipparcos*

TABLE 3
PHOTOMETRY

Star	JD - 2,400,000	Δy	Star	JD - 2,400,000	Δy
HIP 13806.....	52,314.6093	1.4856	HD 26767	52,349.6254	1.4353
	52,315.6109	1.4838	HD 26736	52,328.6250	0.9917
	52,316.6031	1.4782		52,328.6897	0.9903
	52,317.6049	1.4732		52,330.6308	0.9866
	52,327.6049	1.4764		52,332.6253	1.0104
	52,328.6443	1.4800		52,334.6239	1.0016
	52,328.6548	1.4816		52,336.6245	0.9877
	52,330.6054	1.4993		52,338.6183	0.9843
	52,331.5996	1.4975		52,339.6184	0.9997
	52,334.5989	1.4794		52,342.6175	1.0100
	52,336.5999	1.4705		52,345.6350	0.9856
	52,337.5993	1.4762		52,348.6352	0.9948
	52,338.5994	1.4814	HD 26756	52,315.6295	1.8513
	52,339.5992	1.4893		52,316.6226	1.8556
	HD 26767	52,315.6295	1.4323	52,317.6234	1.8442
		52,316.6226	1.4296	52,328.6820	1.8514
	52,317.6234	1.4286	52,330.6221	1.8531	
	52,328.6820	1.4437	52,331.6163	1.8516	
	52,330.6221	1.4425	52,332.6166	1.8533	
	52,331.6163	1.4389	52,336.6171	1.8450	
	52,332.6166	1.4316	52,337.6166	1.8531	
	52,336.6171	1.4395	52,345.6180	1.8487	
	52,337.6166	1.4428	52,348.6278	1.8495	
	52,345.6180	1.4354	52,349.6254	1.8502	
	52,348.6278	1.4384			

shows no obvious periodicity. This is also true for the v_r data sets of these stars observed from Keck, although weak signals may be present for these two stars. However, the P_{rot} is recovered when taking small intervals of Keck v_r data in time for these two program stars. The case of HIP 13806 is different; we found a strong period at 9.60 days (FAP of 0.02%) in the full *Hipparcos* data set. The periodogram peak is sufficiently wide that it encompasses P_{rot} derived from both v_r and Δy . Thus, P_{rot} is somewhat poorly defined from the *Hipparcos* observations alone. The phase curve for the HIP 13806 *Hipparcos* data with a 9.42 day period is shown in Figure 2. HIP 13806 is unusual in that the same period seems to be more or less coherent, although quite noisy, over the ~ 2.5 yr time frame of the *Hipparcos* observations. HIP 13806 is also notable in that it is one of few dwarf stars that show this long-term stability of active regions. Toner & Gray (1988) also observed the G8 dwarf star ξ Boo A, which shows a coherent period over the course of four observing seasons. Certainly, this activity is unusually stable.

3.2. Determination of $v \sin i$ and i

We determined the projected stellar rotational velocity ($v \sin i$) for each of these stars using the radial velocity “template” spectra (observed without the I_2 cell in place) obtained during the Keck observing runs. Using the newest version of the LTE line analysis code MOOG (Sneden 1973), we first derived stellar parameters⁷—effective temperature (T_{eff}), surface gravity ($\log g$), microturbulence (ξ), and metallicity ($[\text{Fe}/\text{H}]$)—for these four stars with interpolated⁸

atmosphere models based on the 1995 version of ATLAS9 code (Castelli, Gratton, & Kurucz 1997). We used no convective overshoot in the model atmospheres. We measured equivalent widths of about 20 unblended Fe I lines and 10 unblended Fe II lines for each star in the region 4490 to 6175 Å (line list provided in Paulson et al. 2003). In a self-consistent manner, gf values for each line were derived from the Kurucz solar atlas (Kurucz, Furenlid, & Brault 1984) and confirmed with a solar spectrum taken through HIRES. The stellar parameters derived are listed in Table 4. The average $[\text{Fe}/\text{H}]$ values listed are relative to solar [$\log \epsilon(\text{Fe}/\text{H})_{\odot} = 7.52$; Sneden et al. 1991]. Using these parameters, we then synthesized a spectral region with five Fe I lines in the region 6150–6180 Å. In order to determine $v \sin i$, we compute a disk intensity profile and then convolve that with a broadening function. This broadening function contains not only $v \sin i$, but also a macroturbulent velocity and an instrumental broadening. We also incorporate into it a limb-darkening coefficient. We used a Gaussian profile to fit the lines of the thorium-argon (ThAr) lamp. We found that a FWHM of 0.09 Å defines the instrumental broadening for this spectral region. The FWHM varies from 0.0918 to 0.0921 Å from the redmost to the bluemost lines, and the synthesis code is insensitive to this small of a change. We estimated macroturbulence (ζ) according to Saar & Osten (1997) for active stars and using $B-V$ from Allende Prieto & Lambert (1999). Using estimates of limb darkening from Gray (1992), we were able to derive $v \sin i$ to within about 0.7 km s^{-1} .

We estimated stellar radii (R_*) from Gray (1992) using derived T_{eff} values, although we acknowledge that the stellar radii will be somewhat increased by the higher metallicity of the Hyades. Metal enrichment increases the opacity in the convection zone. According to hydrostatic equilibrium, as opacity is increased, the change in pressure as a function of optical depth will decrease, causing a slightly larger radius.

⁷ A detailed analysis of the determination of stellar parameters and abundances is provided in Paulson et al. (2003). A shortened description is provided here.

⁸ Interpolation software was kindly supplied by McWilliam (1995, private communication) and updated by I. Ivans (2002, private communication).

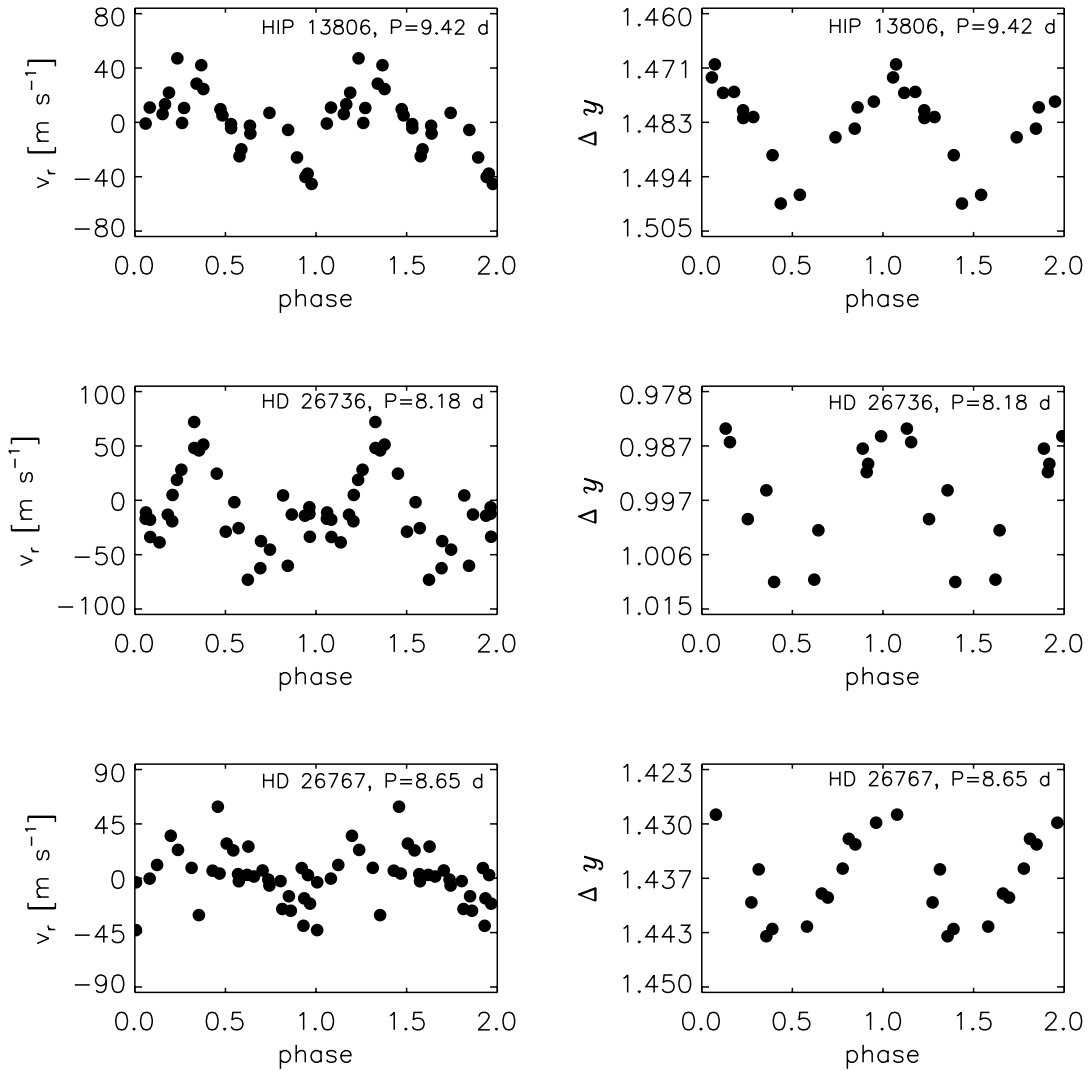


FIG. 1.—Program stars: v_r (left) and differential Strömgren y (right) curves.

For the purposes here, an estimate of R_* based on solar metallicity will suffice.

Using P_{rot} measured from this work, we were able to estimate the rotational axis inclination (i) of each star. The $\sin i$ values are listed in Table 4. Adopting generous errors of 0.3 days for P_{rot} and $0.05 R_\odot$ for R_* and model-dependent errors of 100 K for T_{eff} , 0.3 km s^{-1} for ζ and 0.1 km s^{-1} for ξ , we note that the determination of $\sin i$ is known to within 17% for HD 26736 and HD 26767 and 24% for HIP 13806.

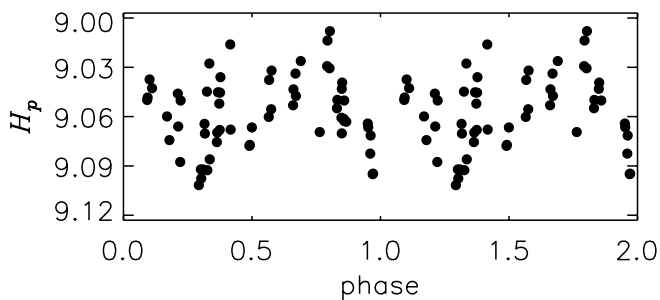


FIG. 2.—Hipparcos photometric data (H_p) for HIP 13806, phased to 9.42 days.

The value of i is useful in indicating the most probable plane for planetary orbits, flagging possible planet occultation candidates (although errors on i make this a blunt tool), and giving the general orientation of the star (guiding first-guess positions for the location of active regions).

4. MODELING v_r VARIATION DUE TO SPOTS AND PLAGE

4.1. Simple Estimates of v_r Variation due to Spots

It is interesting first to compare our results with prediction from the models of Saar & Donahue (1997). The v_r amplitude (A_s) due to a single spot is $A_s \approx 6.5 f_s^{0.9} v \sin i$, where $f_s \approx 0.4 \Delta V$ if we assume spot latitude of 0° , $\sin i = 1$, and an average limb-darkening coefficient of 0.6. ΔV is the photometric amplitude in the V filter (here, we use the photometric amplitude in the Strömgren y filter as an approximate substitute). We list f_s and A_s in Table 4. Figure 3 shows our results for A_s , the predicted amplitude of v_r due to spottedness, versus the observed K velocity amplitude. Note that the A_s values are about a factor of 2 lower than K ($\langle K/A_s \rangle = 2.0 \pm 0.3$). A very small part of this disagreement may come from the use of the y filter as opposed to the V filter, but we believe most of difference arises for two reasons. First, the Saar & Donahue (1997) spot

TABLE 4
 STELLAR PARAMETERS

Star	vB No.	T_{eff} (K)	$\log g$	ξ (km s ⁻¹)	[Fe/H]	ζ (km s ⁻¹)	$v \sin i$ (km s ⁻¹)	$\sin i$	f_s (%)	A_s (m s ⁻¹)
HIP 13806.....	153	5150	4.5	0.60	0.19	2.3	3.8	0.91	1.10	27
HD 26767	18	5900	4.4	0.80	0.23	3.9	5.4	0.83	0.60	21
HD 26736	15	5750	4.4	0.80	0.19	3.8	5.4	0.94	1.00	39
HD 26756	17	5650	4.4	0.80	0.17	3.5	4.5	...	0.44	13

models we used predict the maximum contribution v_r for a given f_s (due to a single, equatorial spot on a $\sin i = 1$ star). Considering multiple spots with the same total f_s or a different $\sin i$ (§ 3.2) will only reduce the predicted A_s further. However, the f_s values we used were *also* derived assuming single spots; thus, the true f_s may be larger than Table 4 suggests. In the general case of multiple spots, one must model the full Δy and v_r curves. Beyond this, the presence of significant amounts of plage on our targets (as implied by, e.g., Ca II H and K emission; Radick et al. 1987) indicates another possible source of v_r fluctuations. Thus, we must consider the possibility of multiple spots and plage contributing to the complex v_r curves.

Based on the above argument, in the case of multiple spots, relations connecting the rms scatter in Δy and v_r might be more useful than the amplitude. Although the data are still limited, there appears to be a trend between the rms scatter in Δy (σ_y) and the rms v_r (σ_v). Figure 4 shows σ_v versus σ_y of the observed data, including HD 166435, HD 19632, and HD 192263. A simple linear least-squares fit yields $\sigma_v(\text{m s}^{-1}) = 3600\sigma_y + 2.29$. Since when $\sigma_y = 0$ this implies $\sigma_v \approx 2.3 \text{ m s}^{-1} \approx \sigma_i$, the internal error of the v_r data, the fit further supports the idea that much of the σ_v in these stars is due to spots.

4.2. Modeling the v_r Effects of Spots and Plage

The effects of dark starspots on the measured v_r have been studied by Saar & Donahue (1997), Hatzes (1999, 2002). Plage, areas of relatively strong magnetic fields and activity that are optically bright, pose greater difficulties for modeling.

Unlike spots, where the dominant effect is simply a strong reduction in the local continuum, in plage the alteration of normal convective motions by strong magnetic fields is not hidden from view by low surface brightness. To model the effects of plage, we use the models presented in Saar (2003). Briefly, we use observed solar bisectors taken in plage and quiet regions at several limb angles as proxies for the bisectors of stellar intensity profiles, I_ν . These proxies were then used to “warp” and shift symmetric I_ν profiles computed in a simple Milne-Eddington model atmosphere. We then employed the now asymmetric quiet and plage I_ν values to construct model stellar flux profiles for stars with any desired $v \sin i$, orientation, and plage geometry. Spots were modeled similarly, except that profiles inside spots were assumed to be symmetric. The centroid of the resulting profile was used to define v_r for the model.

We do not intend to present here a rigorous analysis of the spot and plage contributions to v_r ; this is left for a future paper. Our aim is only to (1) show that simple spot/plage models can explain details of the radial velocity, y , and H α variation beyond merely their amplitude and rms and (2) argue that it is thus *plausible* that spot and plage contribute significantly to the observed Δv_r variations. Our best-fit solutions are not unique and are only indicative of a class of viable solutions under our chosen set of (hopefully physically reasonable) simplifying assumptions. Since the data are also taken over an extended period (~ 4 months), the best-fit parameters necessarily

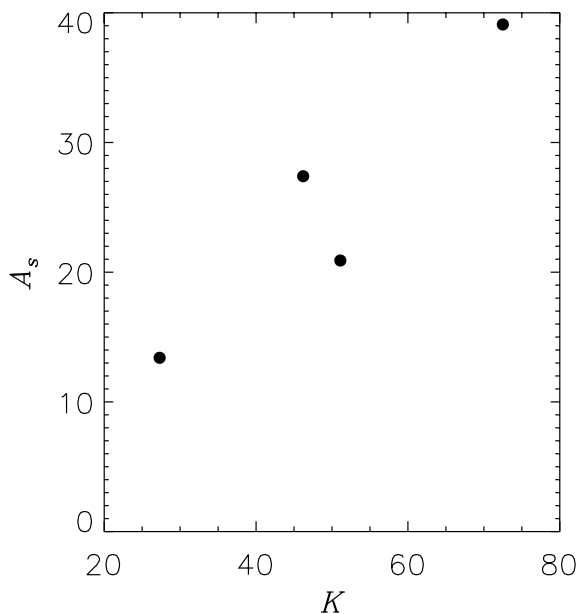


FIG. 3.—Plot of v_r amplitude, A_s , as predicted from Saar & Donahue (1997) vs. K for our program stars.

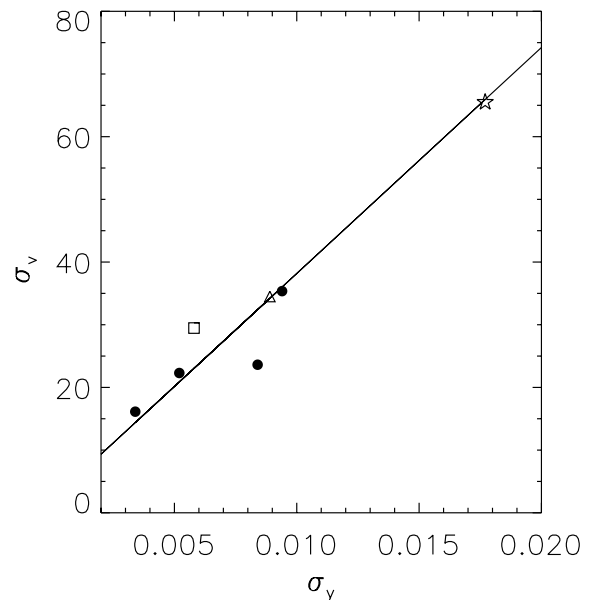


FIG. 4.—Plot of v_r rms vs. y rms for our program stars (circles), HD 166435 (Queloz et al. 2001; star), HD 19632 (G. W. Henry & P. Butler 2002, private communication; box), and HD 192263 (Henry et al. 2002; triangle).

represent time averages of the related physical properties. This is not entirely unrealistic: active longitudes on active stars are known to persist for years (e.g., Jetsu 1996), and even solar active longitudes can be quite long-lived (Berdyugina & Usoskin 2003). Time averages therefore do have some relevant physical meaning. Since the plage models are based on solar line bisectors, we focused on the most solar-like of our Hyad targets, HD 26736.

Our assumptions are as follows. The most significant one is that the spot/plage reside at latitudes $\theta = 30^\circ$ (near the sub-observer $\theta \approx 20^\circ$ for HD 26736), which yields close to the maximum effect for a given region area. We adopt a spot temperature of $T_s = 4000$ K (similar to the Sun), corresponding to a fractional continuum difference in spots at 5000 \AA (relative to the quiet photosphere) of $\Delta I_S = (I_Q - I_S)/I_Q = -90\%$. Additionally, for simplicity, we took the fractional continuum difference in plage (also relative to the quiet photosphere) to be $\Delta I_P = (I_Q - I_P)/I_Q = 0$. A linear limb-darkening coefficient $\epsilon = 0.6$ was adopted, and the regions were assumed circular.

We first attempted to model the observed Δy from HD 26736, successively adding features of varying radius and longitude to fit Δy . Since we have adopted $\Delta I_P = 0$, spots must completely account for the observed Δy . We then apply the resulting spot sizes and positions to compute a model for spot-induced v_r variation. By not *fitting* v_r but rather letting the observed Δy drive the modeling, we ensure that the resulting v_r model is consistent with Δy but does not attempt to “explain” features that are not due to spots. For our assumed θ , a single spot spans only a phase range $\delta\phi \approx 0.5$ (Fig. 5a) and thus cannot alone describe the photometry. The Δy variation

could be reasonably well described with two features [see Table 5 for their properties; fit rms $\sigma_{\text{fit}}(y) = 0.00394$]. We find an optimum “background” unmodulated brightness of $\Delta y = 0.988$ (due to the pristine photosphere plus any uniform spot component). The resulting v_r model agrees fairly well for $\phi > 0.85$ and $\phi < 0.4$, but there are some discrepancies elsewhere. The discrepancies are strongest around phase $\phi = 0.75$, where the differences between v_r and the spot-only model are $\approx 50 \text{ m s}^{-1}$. Adding a third spot could partly correct this, only to introduce new fitting errors to v_r around $\phi = 0.9$ and errors in Δy near $\phi = 0.6$.

The remaining systematic differences between the spot-only model and v_r could be due to plage, our assumptions (especially the restriction on θ), or even potentially a planet. To investigate the first possibility, it is useful to have a plage diagnostic analogous to Δy . Since our HET spectra do not contain the traditional plage indicator Ca II H and K, we constructed a substitute from the H α profile as follows. First, telluric features were removed by ratioing the HD 26736 data with a scaled spectrum of a rapidly rotating A star, whose broad H α feature was removed with a cubic spline fit. The average flux in a 2.15 \AA interval centered on the H α core was then ratioed with the average flux in a nearby, nearly line-free “continuum” segment (5 \AA centered at 6602 \AA) to form an H α index $S_{\text{H}\alpha} = F_{\text{H}\alpha\text{core}}/F_{\text{con}}$. This index showed a small but significant modulation at P_v (Fig. 5b). Comparison of Figures 5a and 5b reveals that the plage emission areas are not coincident with the spots: the $S_{\text{H}\alpha}$ curve maximum is shifted from the Δy minimum, and there are features in $S_{\text{H}\alpha}$ not obvious in Δy (e.g., the enhancement near $\phi \approx 0.9$).

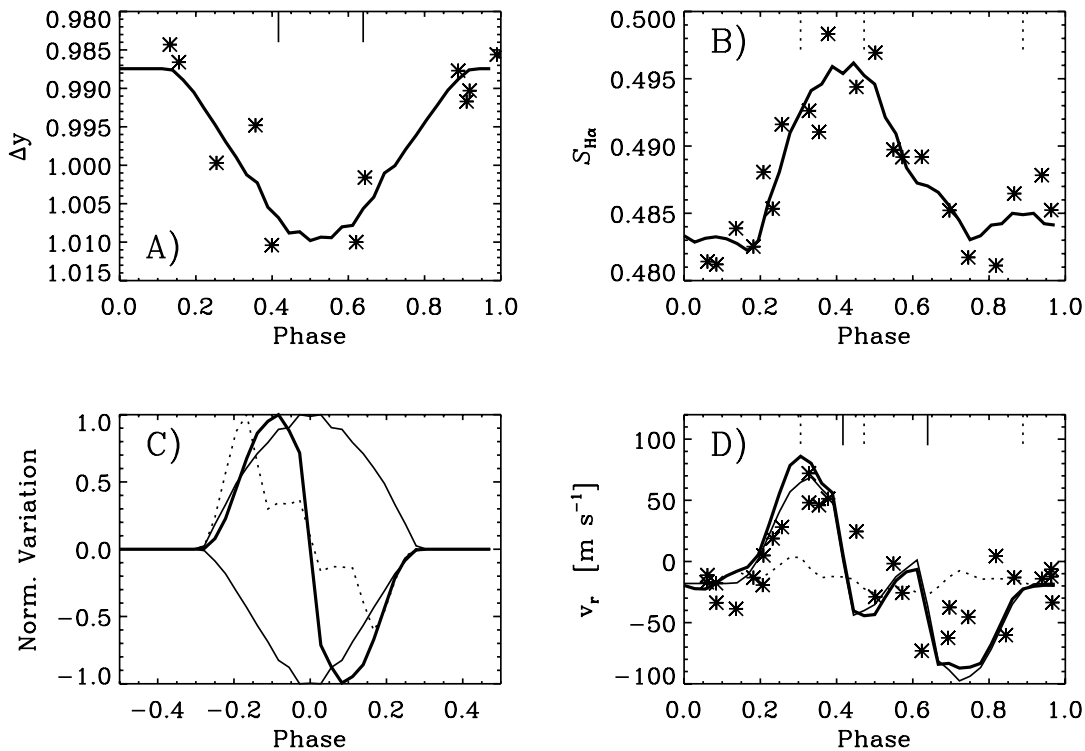


FIG. 5.—Observed Δy , $S_{\text{H}\alpha}$, and v_r for HD 26736 plus models (see Table 5 for model parameters, text for details). (a) Observed Δy (stars), best-fit two spot model for Δy (solid line; $\sigma_{\text{fit}} = 0.00394$), with phase of model spot meridian passage marked (vertical ticks). (b) $S_{\text{H}\alpha}$ computed from observed H α profiles (stars), best-fit three-plage model for $S_{\text{H}\alpha}$ (solid line; $\sigma_{\text{fit}} = 0.00219$), with phase of plage meridian passage marked (vertical ticks). (c) Normalized variation for a single spot v_r (heavy solid line), Δy (solid line), single plage v_r (heavy dashed line), and $S_{\text{H}\alpha}$ (dashed line). Maximum amplitudes are 25.5 m s^{-1} and 0.0112 mag for a $f_S = 1\%$ spot and 3.0 m s^{-1} and $0.0128 \text{ H}\alpha$ units for a $f_P = 1\%$ plage. (d) Observed v_r (stars), v_r of the two spot model that best fits Δy in (a) (solid line; $\sigma = 29.0 \text{ m s}^{-1}$), v_r of the three-plage model that best fits $S_{\text{H}\alpha}$ in (b) (dotted line), and the v_r of the combined spot plus plage model (heavy solid line; $\sigma = 29.1 \text{ m s}^{-1}$). Vertical ticks (top) mark phase of central meridian passage of model spots (solid line) and plages (dashed line).

TABLE 5
SPOT AND PLAGE PARAMETERS: HD 26736

Region	ϕ_0	Area (%)
Spot 1.....	0.42	1.15
Spot 2.....	0.64	1.05
Plage 1.....	0.31	1.15
Plage 2.....	0.47	2.30
Plage 3.....	0.89	1.30

Next, in a fashion similar to the spot-modeling, we added plage regions until the $S_{H\alpha}$ data was reasonably well fitted. We assumed that the $H\alpha$ emission is limb-brightened with $\epsilon = -0.2$. An estimate for the intrinsic plage emission strength per unit area, $I_{S(H\alpha)}$, was also needed. There has been relatively little work using $H\alpha$ as an activity diagnostic in low-to-moderate activity G and K stars. Herbig (1985) found the minimum flux for an early G star in a 1.7 Å bandpass under the $H\alpha$ core (expressed as an equivalent width) is $W_\lambda \approx 0.74$ Å. His most active target, ξ UMa B (G5 V, $P_{\text{rot}} = 3.98$ days), observed with a slightly different bandpass, showed $\Delta W_\lambda \approx 0.277$ Å above this baseline level. If we assume the latter represents a “saturated” chromosphere star ($f_p \approx 1$) and the former a completely inactive star ($f_p \approx 0$), we find (after correcting for resolution and bandpass differences) $I_{S(H\alpha)} \approx 0.016$ for a plage at disk center with an area of 10% of the visible surface. With these assumptions, we found good fits were found for a “background” $S_{H\alpha} = 0.475$ (due to the photospheric $H\alpha$ and any uniform plage/network component). We note, however, that there is a trade-off between plage brightness and area, i.e., fits to $S_{H\alpha}$ are equivalent for $I_{S(H\alpha)} \Sigma f_p \approx \text{constant}$. Thus, changes in $I_{S(H\alpha)}$ affects plage areas and thereby the plage contribution to v_r . A minimum of three regions were required [see Table 5; $\sigma_{\text{fit}}(S_{H\alpha}) = 0.00219$]; the positions of the model spots and plage are also indicated in Figure 5. The resulting plage-induced Δv_r ends up being rather small relative to the spot contribution (model amplitudes of $A_P \approx 16$ m s⁻¹ compared with $A_S \approx 83$ m s⁻¹; Fig. 5d). The inclusion of the plages (at $\theta = 30^\circ$) does not significantly alter the agreement between the resulting v_r model and the data: the rms between them is $\sigma = 29.1$ m s⁻¹. Including plage makes the agreement slightly worse around $\phi \approx 0.1$ – 0.3 by the plage, but slightly better near $\phi \approx 0.5$ – 0.7 ; significant discrepancies remain (Fig. 5d). Whether these discrepancies show any systematic trends (suggesting a possible underlying planetary signal) must await more rigorous modeling, in particular relaxing the assumption of $\theta = 30^\circ$ for all regions. We leave this for a future paper.

5. DISCUSSION AND CONCLUSIONS

This initial search for short-period planets in the Keck Hyades survey has instead turned up several lines of evidence pointing to v_r variations driven by magnetic activity. First, the photometric and the v_r variations show similar periodicities (Fig. 1; Table 1); the one star studied here in $H\alpha$ (HD 26736) shows a similar periodicity in that activity diagnostic as well (Fig. 5b). The v_r amplitudes increase with the Δy photometric amplitudes in a way consistent with (although smaller than) predictions of a simple single-spot model (Saar & Donahue 1997, Fig. 3). The rms scatter in Δy and v_r also show a linear relationship (Fig. 4). This correlation is potentially quite useful as a simple way of estimating σ_v from photometry. More data must be collected before we can predict σ_v from σ_y ,

with confidence; the relationship may depend on other properties/parameters. Once refined, though, such a correlation may be of use to rapidly help flag “problem” stars that will require more careful analysis to confirm planets, to screen out such stars from search lists, or to estimate what fraction of a given star’s σ_v is likely due to activity.

The phase shifts between the v_r and Δy curves clearly seen in at least two of the stars (HIP 13806 and HD 26736) are also consistent with a spot origin for much of the v_r variation. To see this, consider that the perturbation from a single, black spot at $\theta = 0$ on a star (with $i = 90^\circ$ and no limb darkening) scales as $\Delta v_r \propto -f_s \sin \phi \cos \phi$ (where ϕ is the phase angle measured from the subobserver meridian $\phi = 0$), while photometry varies as $\Delta y \propto f_s \cos \phi$. The minimum light (at $\phi = 0$) is shifted from the maximum Δv_r (at $\phi = -45^\circ$); the actual shift will depend on details of the limb darkening and active region geometry. HIP 13806 and HD 26736 (Fig. 1) both show this pattern of v_r maxima preceding light minima. The case of HD 26767 is less clear (two v_r near $\phi \approx 0.4$ are discrepant), but if one identifies the primary maximum with the feature near $\phi \approx 0.2$, it also follows the pattern. Queloz et al. (2001) also see this phase shift in HD 166435.

Finally, beyond these more qualitative connections of v_r with spots and plage, we have also demonstrated that the v_r variations can be modeled directly. By first modeling the observed photometry and $H\alpha$ emission and using the inferred spot and plage locations and sizes in simple models of these regions’ v_r properties, we can explain a significant fraction of the v_r variation of vB 15 in detail (Fig. 5). Given internal errors of $\sigma_i(y) \approx 0.003$ (the constancy of the comparison stars) and $\sigma_i(S_{H\alpha}) \approx 0.0025$, our fits to Δy and $S_{H\alpha}$ are reasonably successful with two spots and three plages, respectively ($\chi^2_\nu = 1.7$ and $\chi^2_\nu = 0.8$). The resulting v_r models are less successful in explaining all the velocity variations ($\sigma \approx 29$ m s⁻¹; $\chi^2_\nu \approx 26$) but are able to account for $\approx 50\%$ of the variance in the v_r data. Some of the discrepancies are undoubtedly due to our simplifying assumptions, such as all regions placed at $\theta = 30^\circ$. Some less obvious implicit assumptions (e.g., that all spots and all plages are identical in how they act on v_r , that the solar plage bisectors used as proxies are representative of stellar plage) may also be important. Still, despite the fact that the modeling presented here is simplified and certainly not definitive, we believe that it argues that a combination of spot and plage can explain many of the v_r fluctuations seen in HD 26736. By analogy, we suspect that many of the v_r variation seen in the other targets can be similarly explained by activity. Indeed, the v_r “jitter” in HD 26756 without corresponding Δy changes or strong periodicity might be the result of rapidly evolving plage dominating the v_r perturbations.

Young stars present distinct problems for the search for short-period planets. Our work shows that photometric confirmation along with good activity measurements are a very helpful check to insure the viability of short-period planetary candidates. It is important to note that active stars need not necessarily be excluded from planet searches, since it should be possible (at least in principle) to remove activity-related perturbations from v_r measurements. Saar & Fischer (2000) show that simple correlations between v_r and a plage diagnostic (e.g., $H\alpha$, Ca II H and K) can be effective in removing long-timescale variations in v_r stemming, for example, from magnetic cycle variations in mean plage area. On shorter (rotational) timescales, this might be accomplished by modeling the activity features (as explored here) or by monitoring line shape

changes (e.g., bisectors) as indicators of rotating inhomogeneous features (Saar et al. 2001, 2002; Queloz et al. 2001).

Magnetic activity and hence activity-induced v_r variations will occur on a wide range of timescales (see, e.g., Fig. 11 from Jenkins 2002 showing solar photometric variability extrapolated to stars; also Donahue, Dobson, & Baliunas 1997a, 1997b for stellar Ca II HK variability). It is important to note, however, that most of the strongly *periodic* power will be concentrated on distinct surface/activity timescales: P_{rot} , differential rotation, active region growth/decay, active longitude growth/decay (including “flip-flops”; see, e.g., Jetsu, Pelt, & Tuominen 1993), and magnetic cycle. Planets with orbital periods well separated from these timescales will be much easier to detect and confirm.

The models also indicate the possibility that plage-induced v_r fluctuations without strong, parallel photometric variations must also be considered as possible contributors to v_r signals. Since plage-to-spot area ratios are largest on inactive stars, it is quite possible that plage-induced Δv_r may dominate on these objects.

Quite apart from planet searches, our work suggests the possible use of precision v_r measurements to investigate surface features on cool stars. The v_r variation as a function of rotational phase is distinctly different for spots and plage and shows significantly sharper changes with ϕ than photometry or chromospheric activity (Fig. 5c). This makes high-precision v_r curves a powerful tool for investigating stellar surface structures, and one uniquely suited for the study of plages and slower rotators ($v \sin i \lesssim 12 \text{ km s}^{-1}$), for which Doppler imaging is less useful.

D. B. P. and W. D. C. are supported by NASA grant NAG5-9227 and NSF grant AST 98-08980. S. H. S. was supported by NASA Origins program grant NAG5-10630. G. W. H. acknowledges support from NASA grants NCC 5-96 and NCC 5-511, as well as NSF grant HRD 97-06268. We would like to thank Artie Hatzes and Chris Sneden for many useful discussions and Rob Robinson and Frank Bash for making the time critical observations at HET possible.

REFERENCES

- Allende Prieto, C., & Lambert, D. L. 1999, *A&A*, 352, 555
 Berdyugina, S. V., & Usoskin, I. G. 2003, *A&A*, 405, 1121
 Castelli, F., Gratton, R. G., & Kurucz, R. L. 1997, *A&A*, 318, 841
 Cochran, W. D., Hatzes, A. P., Butler, R. P., & Marcy, G. W. 1997, *ApJ*, 483, 457
 Cochran, W. D., Hatzes, A. P., & Paulson, D. B. 2002, *AJ*, 124, 565
 Cochran, W. D., Tull, R. G., MacQueen, P. J., Paulson, D. B., Endl, M., & Hatzes, A. P. 2003, in *ASP Conf. Ser. 294, Scientific Frontiers in Research on Extrasolar Planets*, ed. D. Deming & S. Seager (San Francisco: ASP), 561
 Donahue, R. A., Dobson, A. K., & Baliunas, S. L. 1997a, *Sol. Phys.*, 171, 191
 ———. 1997b, *Sol. Phys.*, 171, 211
 ESA. 1997, *The Hipparcos and Tycho Catalogues* (ESA SP-1200) (Noordwijk: ESA)
 Gray, D. F. 1992, *The Observation and Analysis of Stellar Photospheres* (Cambridge: Cambridge Univ. Press)
 Hatzes, A. P. 1999, in *ASP Conf. Ser. 185, Precise Stellar Radial Velocities*, ed. J. B. Hearnshaw & C. D. Scarfe (IAU Colloq. 170) (San Francisco: ASP), 259
 ———. 2002, *Astron. Nachr.*, 323, 392
 Hatzes, A. P., et al. 2000, *ApJ*, 544, L145
 Henry, G. W. 1999, *PASP*, 111, 845
 Henry, G. W., Donahue, R. A., & Baliunas, S. L. 2002, *ApJ*, 577, L111
 Henry, G. W., Fekel, F. C., Kaye, A. B., & Kaul, A. 2001, *AJ*, 122, 3383
 Herbig, G. H. 1985, *ApJ*, 289, 269
 Horne, J. H., & Baliunas, S. L. 1986, *ApJ*, 302, 757
 Jenkins, J. M. 2002, *ApJ*, 575, 493
 Jetsu, L. 1996, *A&A*, 314, 153
 Jetsu, L., Pelt, J., & Tuominen, I. 1993, *A&A*, 278, 449
 Kurucz, R. L., Furenlid, I., & Brault, J. 1984, *Solar Flux Atlas from 296 to 1300 nm* (Sunspot, NM: Natl. Sol. Obs.)
 Mayor, M., & Queloz, D. 1995, *Nature*, 378, 355
 Paulson, D. B., Saar, S. H., Cochran, W. D., & Hatzes, A. P. 2002, *AJ*, 124, 572
 Paulson, D. B., Sneden, C., & Cochran, W. D. 2003, *AJ*, 125, 3185
 Queloz, D., et al. 2001, *A&A*, 379, 279
 Radick, R. R., Thompson, D. T., Lockwood, G. W., Duncan, D. K., & Baggett, W. E. 1987, *ApJ*, 321, 459
 Saar, S. 2003, in *ASP Conf. Ser. 294, Scientific Frontiers in Research on Extrasolar Planets*, ed. D. Deming & S. Seager (San Francisco: ASP), 65
 Saar, S., & Osten, R. 1997, *MNRAS*, 284, 803
 Saar, S. H., Butler, R. P., & Marcy, G. W. 1998, *ApJ*, 498, L153
 Saar, S. H., & Donahue, R. A. 1997, *ApJ*, 485, 319
 Saar, S. H., & Fischer, D. 2000, *ApJ*, 534, L105
 Saar, S. H., Fischer, D., Snyder, N., & Smolec, R. 2001, in *ASP Conf. Ser. 223, in 11th Cambridge Workshop on Cool Stars, Stellar Systems, and the Sun*, ed. R. J. García López, R. Rebolo, & M. Zapatero Osorio (San Francisco: ASP), 1051
 Saar, S. H., Hatzes, A. P., Cochran, W. D., & Paulson, D. B. 2002, in *12th Cambridge Workshop on Cool Stars, Stellar Systems, and the Sun*, ed. A. Brown, G. M. Harper, & T. R. Ayers (Boulder: Univ. Colorado Press), 694
 Santos, N. C., Mayor, M., Naef, D., Pepe, F., Queloz, D., Udry, S., & Blecha, A. 2000, *A&A*, 361, 265
 Sneden, C., Kraft, R. P., Prosser, C. F., & Langer, G. E. 1991, *AJ*, 102, 2001
 Sneden, C. A. 1973, Ph.D. thesis, Univ. Texas, Austin
 Toner, C. G., & Gray, D. F. 1988, *ApJ*, 334, 1008
 Tull, R. G. 1998, *Proc. SPIE*, 3355, 387
 Vogt, S. S., Penrod, D., & Hatzes, A. P. 1987, *ApJ*, 321, 496